Original article
DOI: https://doi.org/10.18721/JPM.15410

THE SPECTRAL CHARACTERISTIC OF A MULTILAYER EXTRINSIC FIBER FABRY–PEROT INTERFEROMETER

L. B. Liokumovich ✉, *N. A. Ushakov, A. A. Markvart, E. Yu. Evdokimenko*

Peter the Great St. Petersburg Polytechnic University, St. Petersburg, Russia

✉ leonid@spbstu.ru

Abstract. The paper describes the development of an analytical response model of an extrinsic fiber Fabry – Perot interferometer with a multilayer cavity in case of spectral interrogation. The system of equations allowing to calculate the spectral characteristic $S(\lambda)$ of such interferometer has been derived under assumption of a single reflection from each of the layer surfaces. Moreover, the key parameters of the interferometer, namely, the layer refractive indices, the reflections of coatings, the layer thicknesses and the light loss in layers were taken into account as well. The light propagation inside the interferometer cavity was analyzed in terms of the Gaussian beam model. The features of the frequency analysis of the $S(\lambda)$ oscillations were also considered. As an example, the obtained equations were used for evaluation of a two-layer extrinsic fiber Fabry – Perot interferometer design.

Keywords: extrinsic fiber Fabry – Perot interferometer, spectral characteristic of interferometer, multilayer interferometer.

Funding: The reported study was carried out within the framework of the State Assignment for Fundamental Research (Subject Code FSEG-2020-0024).

Citation: Liokumovich L. B., Ushakov N. A., Markvart A. A., Evdokimenko E. Yu., The spectral characteristics of a multilayer extrinsic fiber Fabry – Perot interferometer, St. Petersburg State Polytechnical University Journal. Physics and Mathematics. 15 (5) (2022) 129–146. DOI: https://doi.org/10.18721/JPM.15410

Научная статья
УДК 535.3, 535-15, 535.417
DOI: https://doi.org/10.18721/JPM.15410

СПЕКТРАЛЬНАЯ ХАРАКТЕРИСТИКА МНОГОСЛОЙНОГО ВНЕШНЕГО ВОЛОКОННОГО ИНТЕРФЕРОМЕТРА ФАБРИ – ПЕРО

Л. Б. Лиокумович ✉, *Н. А. Ушаков*, *А. А. Маркварт*, *Е. Ю. Евдокименко*

Санкт-Петербургский политехнический университет Петра Великого, Санкт-Петербург, Россия

✉ leonid@spbstu.ru

Аннотация. Статья посвящена разработке аналитической модели отклика внешнего волоконного интерферометра Фабри – Перо с многослойным зазором при спектральном опросе. Была получена система выражений для расчета спектральной характеристики S(λ) такого интерферометра с учетом однократных отражений от поверхностей слоев, а также ключевых параметров конструкции: показателей преломления слоев и коэффициентов отражения покрытий, толщин слоев и световых потерь в слоях. Распространение излучения в среде между зазорами интерферометра проанализировано на основе модели гауссова пучка. Рассмотрены также особенности частотного анализа осцилляций S(λ). В качестве примера полученные выражения использованы для расчетов конструкции двухслойного внешнего волоконного интерферометра Фабри – Перо.

Ключевые слова: внешний волоконный интерферометр Фабри - Перо, спектральная характеристика интерферомера, многослойный интерферометр

Финансирование: Работа выполнена в рамках Государственного задания на проведение фундаментальных исследований (код темы FSEG-2020-0024).

Для цитирования: Лиокумович Л. Б., Ушаков Н. А., Маркварт А. А., Евдокименко Е. Ю. Спектральная характеристика многослойного внешнего волоконного интерферометра Фабри – Перо // Научно-технические ведомости СПбГПУ. Физико-математические науки. 2022. Т. 15. № 4. С. 129–146. DOI: https://doi.org/10.18721/JPM.15410

Introduction

Fiber-optic interferometric sensors have been the focus of great attention because they combine the benefits of optical and fiber-optic devices, offering very high resolution [1, 2]. These include sensors based on the extrinsic fiber Fabry–Perot interferometers (EFFPI), with efforts underway to improve these devices for application in practical measuring systems [3, 4]. The devices include a miniature sensing element based on the Fabry–Perot interferometer formed by the end-face of a waveguide (through which radiation is emitted from the source) and a second movable reflecting plane, for example, a membrane, at a distance L from the end face of the waveguide (Fig. 1,*a*). Similar structures with gaps L ranging from several tens to several hundred micrometers are used to construct sensors for measuring pressure and temperature [5], as well as other physical quantities. Two approaches are generally adopted for interrogating such setups: the so-called white-light interferometry [6] and spectral interferometry [7]. We used spectral interferometry in this study: in this case, the spectral characteristic (transfer function) of the interferometer $S(\lambda)$, namely, the output intensity normalized to the input as a function of the wavelength λ, is recorded during the interrogation. This technique is typically performed using interrogators with wavelength-tunable lasers, or devices with a broadband source at the input of the interferometer and an optical spectrometer at its output.

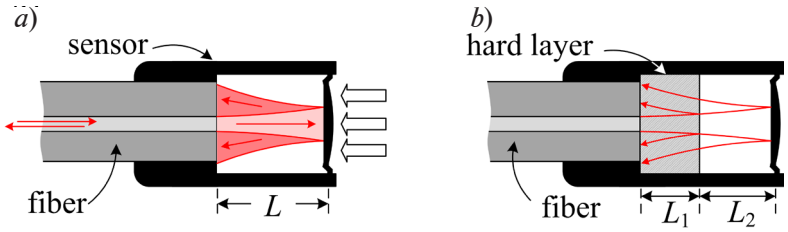

Fig. 1. Scheme of EFFPI-based sensor: regular (*a*), with a two-layer gap (*b*);
L is the thickness of the air gap between the membrane and the fiber endface; L_1 and L_2 are the thicknesses of the hard layer and the air gap; the red arrows indicate the propagation of light beams

A framework for calculating the expected form of the function $S(\lambda)$ is valuable to be able to develop EFFPI-based devices in practice, so that a reliable, validated procedure can be devised for selecting the elements of the optical circuit, estimating the expected sensor parameters, and optimizing the setup. Analyzing the dependence $S(\lambda)$, we can improve the methods for processing it to increase the measurement resolution. Unlike the well-known traditional Fabry–Perot interferometer, divergent radiation propagates in the EFFPI gap, so special non-trivial analysis of this case is required. Analytical consideration of an EFFPI with a single-mode fiber commonly adopts the Gaussian beam model, providing a sufficient description of the function $S(\lambda)$, accounting for the main parameters of the device, primarily the distance L, the refractive index of the medium and its dispersion, fiber parameters, external mirror parameters, wavelength scanning range λ [2, 8–12]. Even though representing the output radiation by a Gaussian beam is an approximation that does not account for reflecting surfaces that are rough/non-flat [13] or for other factors, the dependence $S(\lambda)$ obtained in this case is a good foundation for analyzing and improving practical devices based on EFFPI.

However, parasitic background effects on the measurement results can be a major issue for practical applications of EFFPI-based sensors. First of all, the device should be designed to eliminate the thermal effects, which is problematic. EFFPI with two layers have been adopted for this reason [5, 14, 15] (Fig. 1,*b*). One of the layers with a thickness L_1 is made mechanically rigid and predominantly thermally sensitive. The second layer with a thickness L_2, limited by a movable membrane, is sensitive to pressure, although it is inevitably exposed to parasitic thermal effects. Processing the components of the function $S(\lambda)$ from the first layer, we can assess the temperature changes, accounting for their effect to determine the pressure displacing the membrane.

This method can be further improved if several layers are stacked in the EFFPI gap to measure several quantities at once. Moreover, additional layers in the gap after the fiber end face may be technically necessary for attaching the waveguide in the sensing element.

The calculated dependence $S(\lambda)$ has not been analyzed in the literature for a two- or multilayer EFFPI, unlike the case with the single-layer configuration.

In this paper, we consider a multilayer EFFPI in reflection mode, constructing an analytical model for the spectral characteristic $S(\lambda)$ of such a system.

General structure of interference oscillations for multi-layer EFFPI

It is assumed for the given sensor setup that direct radiation with a certain intensity I_{in}, proportional to the complex electric field strength E_{in}, enters the interferometer via a single-mode waveguide. For certainty, we can assume that this is the intensity and strength of the electromagnetic field on the waveguide axis, since we ultimately intend to analyze the intensity levels normalized by I_{in}. We assume E_{in} to be real, considering its initial phase to be the reference one. The radiation propagating along the waveguide from the interferometer, i.e., reflected from it, is formed by waves of different origin, and the backscatter intensity I takes into account the interference of these reflected waves. The wave reflected directly from the end face of the fiber does not enter the interferometer gap, its complex amplitude E_0 is set by reflection from the interface between the fiber and the medium of the first layer in the interferometer gap. Other reflected waves are formed as radiation enters the interferometer gap, propagates forwards to the boundary with a certain layer in the gap, is reflected from it, passes back to the end face of the fiber and is partially injected into the fiber. The wave formed by reflection from the boundary of the mth layer is denoted as the mth backscattered wave, and its complex amplitude as E_m.

Backscattered waves associated with two or more reflections from the boundaries of the layers are not considered in this case. The first reason for this is that the amplitudes of such backscattered waves in real devices are negligibly small compared with waves from single reflections. Secondly, frequency filtering is typically used to process the spectral characteristics of the interferometer (briefly analyzed below), selecting the fundamental vibrations not associated with rescattering from the boundaries of layers in the interferometer.

The intensity of backscattered radiation is determined by superposition of reflected waves in the waveguide, described by the standard expression:

$$I = \left| \sum_{m=0}^{M} E_m \right|^2 = \sum_{m=0}^{M} \left| E_m \right|^2 + 2 \sum_{m,n} \sum_{m \neq n} \left| E_m E_n \right| \cos\left(\Delta\varphi_{mn} \right), \quad (1)$$

where $\Delta\varphi_{mn}$ is the phase difference of the waves backscattered from the outer boundary of the nth and mth layers (i.e., the difference between the phases Φ_m and Φ_n of complex amplitudes E_m and E_n).

The dimensional constant in expression (1), relating the intensity and the mean-square electric field strength is omitted for simplicity: this is justified because normalization by I_{in} is introduced below. The right-hand side of the expression clearly shows the components describing interference oscillations with varying phase differences $\Delta\varphi_{mn}$.

Since we consider an EFFPI without collimating elements, it is assumed that divergent radiation propagates in the gap, so it is rather difficult to determine the magnitudes of $|E_m|$ and Φ_m at $m > 0$. The level of $|E_m|$ is set by the amplitude of the initial wave E_{in} and a combination of several independent multiplicative factors, which can be written as

$$|E_m| = E_f \cdot T_m \cdot T_{\alpha m} \cdot \eta_m. \quad (2)$$

The factor T_m is associated with the reflection coefficient B_m from the outer boundary of the mth layer and with a decrease in the wave amplitude, corresponding to transmission of layer boundaries in the path of the wave. The factor $T_{\alpha m}$ is associated with optical power losses during propagation in the media filling the interferometer gap in the path of the mth wave. After the light passes through the interferometer gap backwards, only a fraction of its power is 'captured' by the fiber in the form of radiation of its fundamental mode. The coefficient η_m is introduced to account for this. The parameters T_m and $T_{\alpha m}$ are rather simply related to the parameters of the materials and reflective coatings (if the latter are used). However, in the case of an EFFPI with divergent radiation in the interferometer gap, η_m has to be found through analyzing the propagation of radiation and the nature of the wave incident on the end face of the waveguide. In contrast to the phase of the wave E_{in}, the phase delay of the mth backscattered wave in the fiber has to be calculated not only by accounting for the optical path along the gap axis but also by providing a fuller description for the backscattered wave at the fiber end face.

The radiation in the fundamental mode is close to the radiation with a Gaussian intensity distribution and a flat phase front, so the Gaussian beam model with a waist in the fiber end face can be reasonably adopted for propagation of radiation behind the fiber. The width of the Gaussian beam is characterized by the radius W, which varies along the axis of the beam, with its minimum corresponding to the radius of the waist W_0. In the case under consideration, W_0 is given by half the diameter of the waveguide mode spot. While the Gaussian beam is characterized by other parameters, i.e., the curvature of the wavefront R, the Gouy phase φ_G, the Rayleigh length r and the beam divergence θ, in the case of a homogeneous medium, all of them can be recalculated by the value of the waist width W_0 and the distance Z_w from the given point to the waist with the known refractive index of the medium n and the radiation wavelength λ.

The key expressions for describing a Gaussian beam are given in Appendix 1. Expressions have also been formulated for recalculating all the parameters of the beam, if the values of W and R are known at a given point. Moreover, the beam in the given section is fully defined by the so-called complex parameter $q = Z_w + jr$.

The approach based on the Gaussian beam model has become the most widespread for analytical consideration of single-layer EFFPIs [2, 9]. It is assumed here that the beam passes twice the length of the interferometer gap in the forward direction, and in the opposite direction after reflection, remaining Gaussian. The beam has the width W_r and the curvature R_r at the interface with the fiber. The fraction of the radiation power to be 'captured' by the fiber as the radiation of the fundamental mode is determined by the overlap integral of modal field and the radiation incident on the end.

This problem was in fact solved in [16] for a Gaussian beam model with known parameters, considering loss analysis for single-mode fiber splices. This result is also used in exact or extended formulation to describe EFFPI signals.

If the radiation in the EFFPI gap propagates along the waveguide axis, and the outer boundary of the layer is parallel to the end face of the fiber, then the result is described by the expression [9]:

$$\eta = \frac{1}{1+\left(\frac{L_{\mathrm{I}}}{2r}\right)^2}, \quad \Psi = \operatorname{atan}\left(\frac{L_{\mathrm{I}}}{2r}\right), \tag{3}$$

where η is the relative intensity of the radiation injected into the fiber; Ψ is an additional phase shift of the radiation injected into the fiber, added to the phase progression of the wave incident on the fiber end face due to non-uniform transverse phase distribution in the Gaussian beam (see Eq. (A1–1) in Appendix 1); the parameter L_{I} is the distance that the beam has traveled in the interferometer gap; r is the Rayleigh beam length in the medium with the refractive index n filling the interferometer gap, $r = \pi n W_0^2/\lambda$.

In the case of a single-layer EFFPI with a gap thickness L, the radiation path during a single pass through the interferometer is given directly by twice the gap width for $L_{\mathrm{I}} = Z_{w\mathrm{I}} = 2L$. However, if the interferometer gap consists of several layers with different refractive indices, analysis should cover the propagation of radiation through the boundaries of the layers, complicating the problem on the parameters of the beam incident on the end face of the fiber.

Below we analyze the propagation of radiation through the boundaries of the EFFPI layers and determine all the parameters necessary for calculating the intensity of the reflected wave based on expression (1). The analysis is performed based on the Gaussian beam model, assuming that this model remains applicable for propagation of radiation across the layer boundaries. This, in turn, assumes that the conditions for paraxial approximation are satisfied, i.e., beam divergence θ is small. Since $\theta = \lambda_0/(\pi n W_0)$, then, taking the real parameters $\lambda = 1.5$ μm and $W_0 = 5.2$ μm as an example (a standard single-mode waveguide), we obtain a divergence $\theta = 0.092/n$, indicating that it is justified to use the paraxial approximation.

Propagation path of the *m*th wave in a multilayer EFFPI

For simplicity, we assume all the boundaries of the layers to be flat and orthogonal to the beam propagation axis, which is generally consistent with the configuration of real systems. It is necessary to analyze the mth backscattered wave that passes through m dielectric layers, is reflected and travels in the opposite direction. Each ith layer from the 1st to the mth is characterized by the thickness (along the beam axis) L_i and the refractive index n_i. In turn, the value of m can vary from 1 to M, where M is the total number of layers in the EFFPI gap. The wave propagating from the end face of the fiber to the boundary of the mth layer and back passes through $2m - 1$ layers, as illustrated in Fig. 2 with equivalent circuits for unidirectional propagation of waves for the case $M = 3$. In general, the number i changes from 1 to $2(m - 1)$ in a unidirectional equivalent circuit for the mth reflected wave. The reflecting surface in this circuit corresponds to the middle of the mth layer, so the thickness of the layer with $i = m$ is equal to $2L_m$. The z coordinate of the beam cross section in the equivalent circuit is counted from the end face of the fiber. According to the problem statement, the waist of the Gaussian beam at the input to the first layer coincides with the boundary, i.e., with the cross section $z = 0$. Since the second half of the equivalent circuit for unidirectional propagation corresponds to propagation of light in the opposite direction, there is symmetry in the parameters of the circuit's layers. The layer with $i > m$ actually coincides with the layer $2m - i$. Therefore, if $i > m$, we have $L_i = L_{2m-i}$ and $n_i = n_{2m-i}$. However, the beam parameters in the layers, for example, the beam width W_i at the output of the ith layer, do not have such symmetry and need to be calculated.

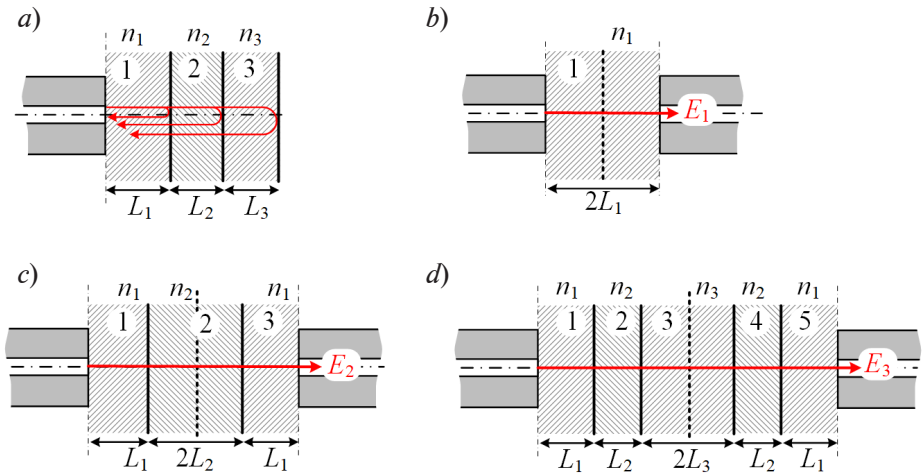

Fig. 2. Backscattered waves in the gap of a three-layer EFFPI ($M = 3$) (*a*) and equivalent single-pass circuits of the 1st (*b*), 2nd (*c*) and 3rd (*d*) waves; $m = 2m - 1 = 1$, the circuit consists of one layer (*b*); $m = 2$, $2m - 1 = 3$, the circuit consists of three layers (*c*); $m = M = 3$, $2m - 1 = 5$, the circuit consists of five layers (*d*)

Propagation of Gaussian beam across the interface between dielectric media

The ABCD matrix model is used to analyze the propagation of light through various optical elements adopting a paraxial approximation [17, 18]. Such a matrix determines the variation in the complex parameter of the beam q for a Gaussian beam. Other parameters of the beam are easily found from the value of q [19]. The radius W and the curvature R of the beam are found from the expressions

$$W = [-\lambda/\pi n \mathrm{Im}(1/q)]^{1/2},\ R = 1/\mathrm{Re}(1/q), \tag{4}$$

then, in view of (4), we can find the distance to the waist and its radius:

$$Z_w = R/[1 + (R/r)^2],\ W_0 = W/[1 + (r/R)^2]^{1/2}. \tag{5}$$

If a Gaussian beam with the parameter q_1 is transformed in some optical element into an output beam with the parameter q_2, then, according to the linear paraxial *ABCD* formalism, the relationship between the output and the input parameters is described by the relation [20]:

$$q_2 = (A \cdot q_1 + B)/(C \cdot q_1 + D),$$

where A, B, C and D are the coefficients of the matrix characterizing the converting optical element.

This approach is often considered in the literature for beams passing through lenses, reflected from mirrors (including spherical ones), and similar cases. However, an *ABCD* matrix for a plane interface between two media (perpendicular to the beam propagation axis). Such a matrix contains the elements $A = 1$, $B = C = 0$, $D = n_1/n_2$ [20].

As a result, we obtain the following expression:

$$q_2 = q_1\,(n_2/n_1). \tag{6}$$

Thus, the beam divergence and the Rayleigh length change as the beam passes through the interface between dielectric media.

The distance from the interface to the waist Z_{w2} for an equivalent beam of the second layer differs from $Z_{w1} = L_1$. The equivalent beam of the *i*th layer here and below refers to a beam that propagates in a homogeneous medium with a refractive index $n = n_i$, completely coinciding with the Gaussian beam considered within the *i*th layer.

If the parameters of the beam in the first medium are known (it is sufficient to set the waist width W_0, n_1, and λ), we can find the complex beam parameter q_{1e} in the cross section $z_1 = L_1$ (the subscript 1 in q_{1e} corresponds to the layer number, the subscript e indicates that the parameter corresponds to the exit (in the propagation direction) boundary of this layer). Next, we can find q_{2b} from expression (6) (the subscript b indicates that the parameter corresponds to the input section of the layer). We can then use expressions (4) and (5) to find the distance from the cross section z_1 to the waist of the equivalent beam of the second layer Z_{w2} as well as the remaining parameters of the beam in the second medium.

There are several important circumstances.

Firstly, if we substitute Eq. (4) into Eq. (5) for W_0, it can be confirmed that the value of W_0 does not change as q is transformed in accordance with (6),, i.e., for the waist radius is also equal to W_0 for an equivalent beam of the second layer,. Since the Rayleigh beam length is equal to $r = \pi n W_0^2/\lambda$, and the divergence $\theta = \lambda/(\pi n W_0)$, we obtain given the same values of W_0 that as the beam passes through the boundaries of layers in the interferometer gap, the Rayleigh length and divergence vary only slightly from one medium to another, in accordance with the refractive index: $r_m = \pi n_m W_0^2/\lambda$, $\theta_m = \lambda/(\pi n_m W_0)$.

Secondly, we should note that Eqs. (6) and (4) give the same values for the beam width at the interface if it is calculated from q_{1e} or q_{2b}. Calculating the value of W at the interface by Eq. (P1-2) (see Appendix 1) with the parameters W_0, n_1 and the argument $Z_{w1} = L_1$ gives the same result as calculating it with the parameters W_0, n_2 and the argument Z_{w2}. This is fully consistent with the physical meaning, since there is no reason for jumps in the beam width at the interface, unlike the jump in the curvature radius corresponding to beam refraction at the interface.

The given change in the parameters of the Gaussian beam as it passes across the interface between two media is illustrated in Fig. 3, showing the variation in the beam in the case when $n_1 > n_2$. The width W_1 (blue line) is calculated by the expression (P1-2) (see Appendix 1) for $W_1(z)$ at $n = n_1$ and corresponds to the actual beam in the first medium (solid line) and the equivalent beam in the second medium (dashed line). In turn, the width W_2 (red line) is given by the expression (P1-2) as

$$W_2(z_2') = W_2(z + Z_{w2} - L_1)$$

for $n = n_2$, corresponding to the actual beam in the second medium (solid line) and its equivalent beam in the first medium (dashed line).

The next step is to analyze the expression for the quantity Z_{w2} that is the distance from the interface between the two media to the waist of the equivalent beam of the second layer. In accordance with expression (6), we find that the complex parameter at the interface from the second layer is expressed as

$$q_{2b} = (n_2/n_1)\cdot q_{1e} = (n_2/n_1)\cdot(L_1 + jr_1).$$

Next, using Eqs. (4) and (5), we obtain the curvature of the beam in the second layer:

$$R_{2b} = \frac{1}{\mathrm{Re}\left(\dfrac{1}{q_{2b}}\right)} = \frac{n_2}{n_1}\cdot\frac{L_1^2 + r_1^2}{L_1}, \tag{7}$$

as well as the distance to the waist of the equivalent beam of the second layer:

$$Z_{w2} = \frac{R_{2b}}{1 + \left(\dfrac{\lambda}{\pi n_2 W_{12}^2} R_{2b}\right)^2}, \tag{8}$$

where the notation $W_{12} = W_{1e} = W_{2b}$ is introduced for the width of the Gaussian beam at the interface between the media.

The value of W_{12} can be found either from expression (4) in terms of q_{2b} or q_{1e}, or directly by Eq. (P1-2) for $z = L_1$ in the form

$$W_{12} = W_0\sqrt{1+\left(\frac{L_1}{r_1}\right)^2}, \tag{9}$$

where r_1 is the Rayleigh beam length in the first layer, $r_1 = \pi n_1 W_0^2/\lambda$.

Next, if we substitute expressions (7) and (9) into Eq. (8), we obtain the following simplified result:

$$Z_{w2} = \frac{n_2}{n_1}L_1. \tag{10}$$

The relationship (10) sets the waist shift of the equivalent beam of the second layer from $z = 0$ to the interface of the layers at $n_2 < n_1$, when beam divergence increases as the beam crosses the interface (this case is shown in Fig. 3). Conversely, the waist of the equivalent beam shifts to the region $z < 0$ at $n_2 < n_1$, when beam divergence decreases as the beam crossses the interface.

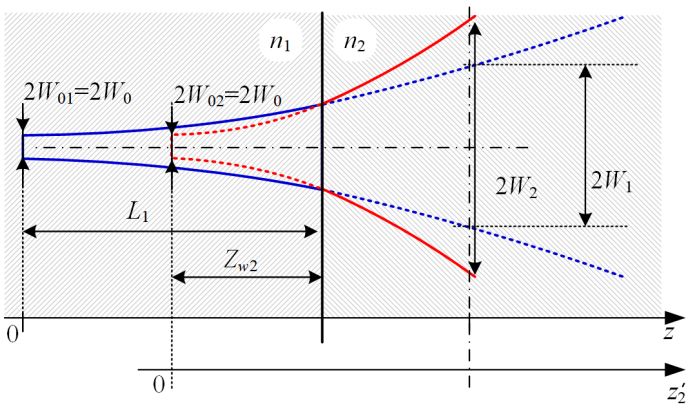

Fig. 3. Variation in the radius of the beam passing from the first to the second medium (case $n_1 > n_2$) for actual beam (solid lines) and for equivalent beams (dashed lines)

Propagation of Gaussian beam through several dielectric media and description of the *m*th backscattered wave in the EFFPI

The expressions obtained above allow to find (within the paraxial approximation) the parameters of the Gaussian beam after it passes across the interface between two dielectric media, and, consequently, to calculate the parameters of the beam at the exit from the second medium. Next, we can similarly consider the beam transformation at the interface between the second and third layers and then generalize the calculation to the case of a sequence of several dielectric layers. Analysis of the general case, i.e., the EFFPI with M layers, should be cover the propagation of a light beam to $2M - 1$ layers. However, there is no need to calculate all the parameters of the beam in different layers, and it is sufficient to apply only the result of Eq. (10). Indeed, we can consider an equivalent beam instead of a real one at the interface with the third layer, propagating in a medium with the refractive index $n = n_2$ with the waist W_0 at a point at a distance $Z_{w2} + L_2$ from the interface between the second layer and third layer. Performing the same calculations as before for the boundaries of the second and third layers, we can confirm that the result for the distance from the boundary to the waist of the equivalent beam of the third layer is absolutely equivalent to that expressed by Eq. (10), specifically,

$$Z_{w3} = \frac{n_3}{n_2}\left(Z_{w2} + L_1\right). \tag{11}$$

If we substitute expression (10) into Eq. (11), we obtain:

$$Z_{w3} = \frac{n_3}{n_2}\left(\frac{n_2}{n_1}L_1 + L_2\right) = n_3\left(\frac{1}{n_1}L_1 + \frac{1}{n_2}L_2\right). \tag{12}$$

Generally speaking, it is evident for a Gaussian beam propagating into the ith layer that the distance from its boundary with the $(i-1)$th layer to the waist of the equivalent beam of the ith layer is given by the expression

$$Z_{w3} = n_3\left(\frac{1}{n_1}L_1 + \frac{1}{n_2}L_2 + \ldots + \frac{1}{n_{i-1}}L_{i-1}\right). \tag{13}$$

The mth reverse beam in the given multilayer interferometer in reflection mode passes through $2m-1$ layers with the symmetry shown in Fig. 2. After returning to the input point, we obtain the distance $Z_{w(2m-1)}$ to the waist of the equivalent beam passing through the first layer in the opposite direction. The total distance L_{1m} from the waist of the equivalent beam of this layer to the fiber boundary on which the beam is incident is $Z_{w(2m-1)} + L_1$.

In view of expression (13), we obtain:

$$L_{\mathrm{Im}} = 2\left(L_1 + \sum_{i=2}^{m}\frac{n_1}{n_i}L_i\right). \tag{14}$$

The resulting expression (14) can be substituted into Eq. (3), yielding the key parameter h

$$\Phi_m = \left(\frac{4\pi}{\lambda}\sum_{i=1}^{m} n_i L_i\right) + \varphi_{\mathrm{G}}\left(L_{\mathrm{Im}}\right) + \varphi_{rm} + \Psi\left(L_{\mathrm{Im}}\right), \tag{15}$$

where the term φ_{rm} denotes an additional phase shift that may occur upon reflection from the boundary of the mth layer and depending on the nature of this reflection.

The phase shift $\Psi(L_{1m})$ for the fiber mode excited by a Gaussian beam incident on the end face is given by expression (3).

The last and relatively simple factor in Eq. (2) for the magnitude of $|E_m|$ required to calculate the intensity (1) reflected from the EFFPI is the multiplier T_m. It accounts for the variation in the amplitude of the wave passing through the interferometer gap. Considering the sequence in which the Gaussian beam passes through the boundaries and the reflection for the mth wave, we can easily obtain the following expression for the multiplier T_m:

$$T_m = B_m \cdot \prod_{i=0}^{m-1}\left(1 - B_i\right)^2. \tag{16}$$

As mentioned above, B_m is the reflection coefficient from the outer boundary of the mth layer, i.e., the boundary of the mth and $(m+1)$th layers. The coefficient $T_0 = B_0$ for the wave E_0, i.e., it is equal to the reflection coefficient from the fiber end face. If the reflections are related only to the difference in the refractive indices of the layers, then the reflection and transmission coefficients are determined by Fresnel reflections and expression (16) for this case has the form

$$T_m = \prod_{i=0}^{m}\frac{4n_i n_{i+1}}{\left(n_i + n_{i+1}\right)^2},\ B_m = \frac{\left|n_m - n_{m+1}\right|}{n_m + n_{m+1}}, \tag{17}$$

where, as we recall, n_0 is the refractive index in the core of the fiber.

Expression (2) accounts for considerable light absorption occurring in the layers by a multiplier taking the form

$$T_\alpha = \prod_{i=1}^{m-1} \alpha_i^2 = \prod_{i=1}^{m-1} 10^{-\alpha_i L_i/10}, \tag{18}$$

where a_i are the amplitude transmission coefficients of the layers (the square power accounts for forward and backward propagation through the layers.

The transmission coefficients in the right-hand side of Eq. (18) are expressed as linear losses α_i (in dB per unit length).

The expressions obtained above describe all the components necessary for calculation by expression (1).

Spectral characteristic of the EFFPI

Expression (1) and detailed description of its components provides the general structure for the model of interference oscillations occuring at the output of the EFFPI. As already noted, interrogation of such structures in measuring devices is generally carried out by methods of spectral interferometery. In this case, the so-called spectral characteristic (transfer function) of the interferometer $S(\lambda)$ is recorded and analyzed. It is defined as the dependence of the intensity of light reflected from the EFFPI (relative input level) with the wavelength λ varying in the operating range $\Delta\lambda$ centered at the wavelength λ_0. Evidently, the spectral characteristic of a multilayer EFFPI can be found by expression (1) if $E_{in} = 1$ and it is assumed that the quantity λ is variable. In this case, it is convenient to analyze $S(\lambda)$ as a sum of a quasi-constant component and oscillating components

$$S(\lambda) = S_0(\lambda) + \sum_{m,n}\sum_{m\neq n} S_{mn}(\lambda), \tag{19}$$

where

$$S_0(\lambda) = \sum_{m=0}^{M} |E_m|^2,\ S_{mn}(\lambda) = 2|E_m E_n|\cos(\Delta\varphi_{mn}). \tag{20}$$

The component I_0 slowly changes with the wavelength λ, mainly due to the variation in the ratio $L_{\mathrm{I}m}/r_1$ included in the coefficient η_m, which sets the amplitude of the mth wave. The oscillating components I_{mn} describe the interference oscillations of the mth and nth backscattered waves. The amplitude of such a component $|E_m E_n|$ also varies depending on λ for the above reasons. Nevertheless, a larger contribution is made by the oscillations determined by the variation in the argument $\Delta\varphi_{mn}$ depending on λ, which can be represented by different components:

$$\Delta\varphi_{mn} = \Phi_m - \Phi_n = \frac{4\pi l_{mn}}{\lambda} + \varphi_{\mathrm{G}mn} + \varphi_{rmn} + \Psi_{mn}, \tag{21}$$

where l_{mn} is the optical difference of the progression of the mth and nth interfering waves.

In view of sum (15), the difference l_{mn} follows the expression

$$l_{mn} = \sum_{i=1}^{m} n_i L_i - \sum_{i=1}^{n} n_i L_i. \tag{22}$$

The other components of Eq. (21) are determined by the differences

$$\begin{gathered} \varphi_{\mathrm{G}mn} = \varphi_{\mathrm{G}}(L_{\mathrm{I}m}) - \varphi_{\mathrm{G}}(L_{\mathrm{I}n}), \\ \varphi_{rmn} = \varphi_{rm} - \varphi_{rn}, \\ \Psi_{mn} = \Psi(L_{\mathrm{I}m}) - \Psi(L_{\mathrm{I}n}). \end{gathered} \tag{23}$$

It is assumed for the case $m = 0$ that the sum with the limit m in expression (22) is equal to zero; the first equation in system (23) implies that

$$\varphi_G(L_{I0}) = \varphi_{G0} = \Psi(L_{I0}) = 0.$$

If we consider the values of L_i and $\Delta\lambda$ relevant for real-life EFFPIs, we can observe that the variation in the component $4\pi l_{mn}/\lambda$ during wavelength scanning is more significant than that in the components φ_{Gmn}, φ_{rmn} and Ψ_{mn}. Moreover, the component $1/\lambda$ is expressed in the case $\Delta\lambda << \lambda_0$ as

$$1/\lambda \approx 1/\lambda_0 - \delta\lambda/\lambda_0,$$

where $\delta\lambda = \lambda - \lambda_0$ is the wavelength shift relative to the center of the scanning range.

Therefore, the oscillation $S_{mn}(\lambda)$ can be approximately written as

$$S_{mn}(\lambda) \approx 2\left|E_m E_n\right| \cos\left(\frac{4\pi l_{mn}}{\lambda_0^2}\delta\lambda + \varphi_{mn}\right), \tag{24}$$

where the term φ_{mn} includes the sum of the components φ_{Gmn}, φ_{rmn}, Ψ_{mn} and $4\pi l_{mn}/\lambda_0$.

It is preferable to calculate the dependence $S(\lambda)$ using a more rigorous representation of the argument in oscillations (21). On the other hand, approximation (24) clearly demonstrates that the spectral characteristic for wavelength scanning in fact contains quasi-harmonic oscillations, when each pair of backscattered waves with the numbers m and n corresponds to a quasi-harmonic oscillation $\cos(\Omega_{mn}\cdot\delta\lambda)$, with the 'frequency' $\Omega_{mn} = 4\pi l_{mn}/\lambda_0^2$ (the frequency is in quotation marks here because it characterizes oscillations depending on λ and is measured in reciprocal meters).

In general, the properties of the dependence of S on the wavelength λ are set by explicitly including the wavelength into expressions (21) or (24), as well as through its influence on such parameters in the resulting expressions as r_1, φ_G and Ψ (the parameter φ_r can also vary with the wavelength). However, another possible factor affecting the spectral characteristic of the EFFPI is that other parameters of the above expressions may also depend on the wavelength . First of all, consider the dependence of n_m magnitude on the wavelength due to dispersion in the material of the mth layer. While the $n_m(\lambda)$ dependence does not affect the general nature of the variation in $S(\lambda)$, it makes a pronounced contribution to the specific quantitative parameters of the oscillations. For example, the parameter l_{mn}, introduced in expression (22), depends on the refractive coefficients of the layers passed by the mth and nth backscattered waves, so analysis of the actual frequency of 'oscillations' Ω_{mn}, obtained by approximation (24) taking into account the dependence of dispersion in the layers should be, generally speaking, refined (the modifications are partially given below).

Example applications of resulting system of expressions

Let us calculate the dependence $S(\lambda)$ of a two-layer EFFPI with the specified parameters (Fig. 4,*a*). We take the wavelength scanning interval from 1.51 to 1.59 μm (i.e., $\Delta\lambda = 80$ nm) with a step of $\delta\lambda = 40$ pm, typical for modern infrared interrogators. Standard single-mode fiber with a fused-silica core and a mode spot diameter of 10.4 μm was taken. Therefore, we assume that $W_0 = 5.2$ μm and $n_0 = 1.44$. Suppose a silicon layer with a thickness $L_1 = 300$ μm is positioned behind the fiber, and a submembrane air gap with a thickness $L_2 = 105$ μm. The membrane material adjacent to the the air gap should be specified to be definite; we assume that this also silicon for simplicity. The power losses of light in silicon and in the air layer are be neglected, assuming $T_\alpha = 1$. We take $n_2 = 1$ for air, and use the value calculated by the Sellmeyer equation for silicon (see Appendix 2). Eq. (A2-1) yields $n_1(\lambda_0) = 3.478$ in the center of the scanning range, which, according to Eq. (17), gives the power reflection $B_0 = 17.2\%$ at the interface with the fiber and $B_1 = B_2 = 30.6\%$ at the interface with air. The variation Δn_1 of n_1 within the scanning range is $\Delta n_1 = 0.0066$. This variation has little effect on reflections, so we dopt a fixed value of n_0 for silica. However, the variation in n_1 is important for analyzing the frequency shifts of the oscillations (the analysis is presented below), while $n_1(\lambda)$ is calculated taking into account Eq. (A2-1).

Calculation for the case $M = 2$ should take into account three backscattered waves with amplitudes E_0, E_1 and E_2; in this case, the phases φ_r were taken equal to zero. The dependence $S(\lambda)$ calculated in accordance with the structure of Eqs. (19), (20) and taking into account Eqs. (17), (7), (3) is shown in Fig. 4,*b*. According to (19) and (20), it is the sum of one quasi-static and three quasi-harmonic components.

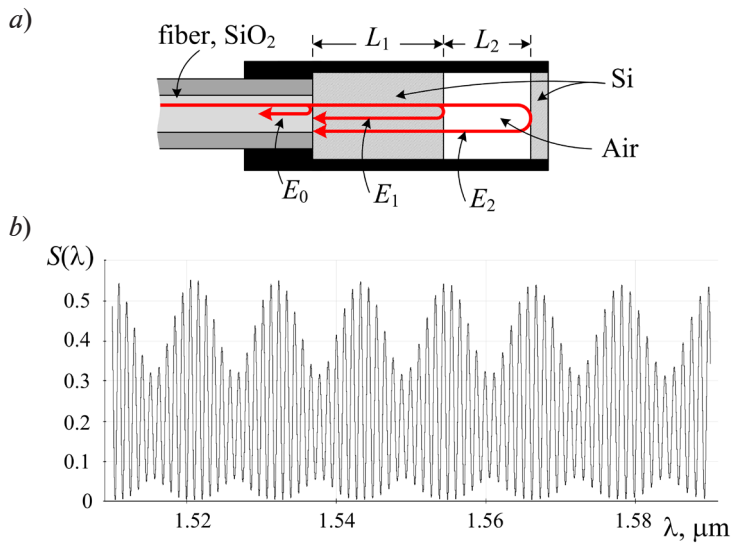

Fig. 4. Setup of two-layer EFFPI (*a*) and the calculated spectral characteristic $S(\lambda)$ for this setup (*b*)

The calculated values obtained for for the center of the scanning range λ_0 are

$$S_0 = 0.240,\ S_{01} = 0.204,\ S_{02} = 0.073 \text{ and } S_{12} = 0.043.$$

The estimated values of oscillation frequencies in this case are

$$\Omega_{01} = 5457.0,\ \Omega_{02} = 6006.2 \text{ and } \Omega_{03} = 549.2\ (1/\mu\text{m}).$$

They correspond to the interference of pairs with progression differences l_1, $l_1 + l_2$ and l_2, so we can formulate the relationship $\Omega_{02} = \Omega_{01} + \Omega_{03}$. The oscillations in Fig. 4,*b* correspond to this sum: while high-frequency beats are very pronounced(this is the sum of the frequencies Ω_{02} and Ω_{01}), the envelope is complex and asymmetric due to the influence of the third term with the frequency Ω_{12}. There are no considerable quasi-static variations, since the above values of S_0, S_{01}, S_{02} and S_{12} for λ_0 vary within a few percent when the wavelength shifts to the edges of the scanning range. The contribution of the phase components φ_{mn} is negligible compared to $4\pi l_{mn}/\lambda$, therefore it is insignificant.

The given calculated example illustrates how the expected characteristic $S(\lambda)$ is obtained for the specific parameters of the device. Apparently, the overall level of output power fluctuations is approximately 60% relative to the input, allowing to coordinate the requirements for the photodetector and the source. Estimating the oscillation frequencies of $S(\lambda)$, we can select the correct parameters for detecting the signal. Obtaining the relative levels of oscillating components, as well as accounting for the noise level and the properties of processing algorithms allow to evaluate the resolution to reliably measure the variation in the optical path lengths of the silicon and air layers. Furthermore, calculating the expected characteristic $S(\lambda)$ and its parameters by this method allows to optimize the parameters of the device within the range available for real devices.

Frequency analysis of spectral characteristics for a multilayer EFFPI

As discussed in Introduction, high-precision measurement methods based on EFFPI can be used to record and process the spectral characteristics of the interferometer $S(\lambda)$. This processing can be rather complex, but it generally involves calculating and analyzing the spectrum $F(\Omega)$ by applying the Fourier transform to the initially recorded dependence $S(\lambda)$. This is necessary for isolating the necessary oscillation component, reducing noise and distortion. In the case of a multilayer interferometer, the primary means for separating the components of different pairs of interfering waves and processing them individually is frequency filtering of $S(\lambda)$ components. Even finding the spectral peak positions of $F(\Omega)$ allows to approximately estimate the required lengths of the layers, since, as follows from Eq. (24), $l_{mn} = \lambda_0^2\Omega_{mn}/4\pi$ (such an estimate does not give high measurement accuracy, which requires more complex processing).

However, several important points should be raised before calculating the spectrum $F(\Omega)$ and performing its preliminary analysis. Previous analysis considered the dependence $S(\lambda)$, since devices for spectral interrogation specifically record the output intensity level of the EFFPI as function of the wavelength in most cases. As noted above, the components of $S_{mn}(\lambda)$ are quasi-harmonic, i.e., different from a strictly harmonic dependence. These differences are also associated with potential variation in the amplitude and phase parameters depending on λ in the expressions obtained, but the strongest deviation is due to the chirp present in the oscillating components. The initial progression of the cosine argument in expression (20) is given by the ratio $4\pi l_{mn}/\lambda$, which is only approximately substituted by a linear shift in a narrow range of $\Delta\lambda$. Therefore, the components $S_{mn}(\lambda)$ in the calculations of the spectrum $F(\Omega)$ are represented, instead of discrete components with frequencies Ω_{mn}, by some broadened lines, possibly of complex shape. Moreover, the higher the value of Ω_{mn}, the stronger the broadening and more difficult it is to process the component $S_{mn}(\lambda)$.

Notably, it is relatively easy to eliminate this difficulty if instead of $S(\lambda)$, we consider the spectral characteristic $S(\nu)$ in the optical frequency range $\nu = c/\lambda$(c is the speed of light in vacuum). Formally substituting the variable in the resulting expressions converts the oscillating components of $S_{mn}(\nu)$ to the form

$$S_{mn}(\nu) = 2\left|E_m E_n\right|\cos\left(\frac{4\pi l_{mn}}{c}\nu + \varphi_{mn}\right), \tag{25}$$

where φ_{mn} includes the sum of the components φ_{Gmn}, φ_{rmn}, Ψ_{mn}, which, like the amplitudes $|E_m|$, are determined by the same expressions as before, but with the substitution $\lambda = c/\nu$.

Expression (25) corresponds to the harmonic dependence on ν and there is no chirp effect for $S_{mn(\nu)}$ oscillations. Therefore, if the Fourier transform is applied specifically to $S(\nu)$, the resulting spectrum of $F(\Omega')$ has clear peaks for the components $S_{mn}(\nu)$ with the 'frequencies' $\Omega'_{mn} = 4\pi l_{mn}/c$ (in this case, the parameter Ω' is measured in Hz^{-1}, i.e., corresponds to the scale of time units).

It is important to emphasize that in practice, this substitution of the wavelength λ with the frequency ν is associated not only with the new variable in the ratio $\nu = c/\lambda$. Spectral interrogators typically generate a sample set $S_i = S(\lambda_i)$, where the values of λ_i are distributed within the scanning range ща $\Delta\lambda$ with a uniform step. The sample set S_i should be resampled by interpolation to correctly apply the discrete Fourier transform to the spectral characteristic of the EFFPI with a modified argument scale; the samples $S'i$ of the transformed set should in this case correspond to a uniform step in frequency ν. The application of the Fourier transform to the sequence S'_i gives a spectrum $F(\Omega')$ with peaks Ω'_{mn}, which correspond to the optical path differences $l_{mn} = \Omega'_{mn}\cdot c/4\pi$.

The ratios $l_{mn} = \lambda_0^2\,\Omega_{mn}/4\pi$ and $l_{mn} = \Omega'_{mn}\cdot c/4\pi$ allow using the scale of optical path difference for the arguments of the spectra $F(\Omega)$ and $F(\Omega')$ by replacing the initial arguments Ω and Ω' with the argument $l = \lambda_0^2\,\Omega/4\pi = \Omega'\cdot c/4\pi$. Then the peak positions of the spectra $F(l)$ and $F(l)$ correspond to the optical path difference of interfering pairs of backscattered waves.

Another important finding follows from representing the spectral characteristic of the EFFPI as a function of ν in the form (25). This form allows to consider the effect of weak dispersion, when the dependence of the refractive index n on the wavelength in the range $\Delta\lambda$ can be described (the same as on the frequency) using a linear correction:

$$n(\lambda) = n(\lambda_0) - n_\lambda' \cdot \delta\lambda.$$

If we substitute this representation for n to Eqs. (22) and (25), taking into account that the frequency varies within the range $\nu_0 \pm \Delta\nu$ ($\nu_0 = c/\lambda_0$) and discard the components with second-order smallness, we obtain that

$$\Omega'_{mn} = \frac{4\pi}{c}\left(\sum_{i=1}^{m} n_{gi}L_i - \sum_{i=1}^{n} n_{gi}L_i\right), \tag{26}$$

where n_g is the group refractive index at the point $\lambda = \lambda_0$;

$$n_g = n(\lambda_0) - \lambda_0\cdot n_\lambda'$$

(for example, this influence of dispersion was discussed for a single-layer EFFPI in [21, 22]).

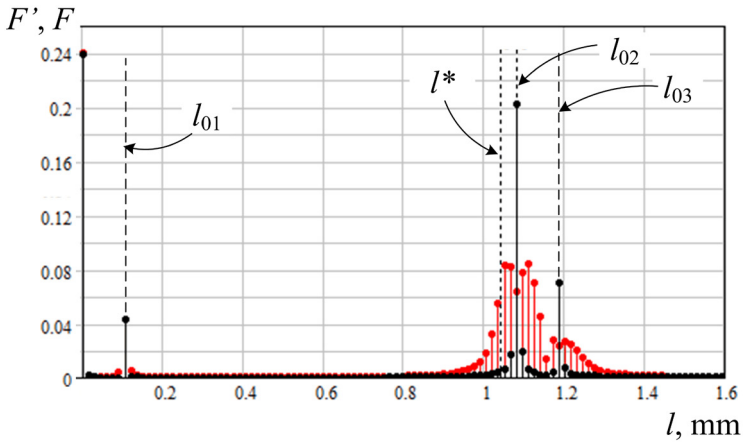

Fig. 5. Computational spectra F' and F with the scale of the argument l (colored in black and red respectively)

As an illustration, we calculate the spectra $F(l)$ and $F'(l)$ for an EFFPI with the setup described above (see Fig. 4,*a*). The calculated characteristic $S(\lambda)$ for this setup is shown in Fig. 4,*b*. According to the values adopted for $\Delta\lambda$ and $\delta\lambda$, this characteristic was a set of 2,000 samples S_i. After using spline interpolation to recalculate these samples into a scale with a uniform frequency step ν and applying the Fourier transform, as well as substituting $\Omega' = 4\pi l/c$, we obtain the spectrum F' with the scale of the argument l (Fig. 5). Notably, if the spatial resolution given by the range $\Delta\lambda$ is recalculated by the scale of the argument l, it amounts to $\delta l = 7.5$ μm. The resulting spectrum $F'(l)$ contains one constant component and three components with positions that exactly coincide with $l_{12} = L_2 = 105$ μm (it is taken into account here that $n_2 = 1$),

$$l_{01} = n_{g1} L_1 = 1.082 \text{ mm}, \; l_{02} = n_{g1} L_1 + L_2 = 1.187 \text{ mm}.$$

Evidently, the amplitudes coincide for all four components of the spectrum $F'(l)$ and the above values of S_0, S_{01}, S_{02} and S_{12} for λ_0. Minor discrepancies can be associated with insufficient resolution δl, which is why the calculated points l may not coincide with the exact position of the spectral peak. Fig. 5 also shows the position

$$l^* = n_1(\lambda_0) L_1 = 1.043 \text{ mm}.$$

Evidently, the estimate l^* is very different from the actual position l_{01}, suggesting that dispersion should be taken into account, as discussed above.

In addition, the red lines and symbols in Fig. 5 show the results for $F(l)$ calculated by Fourier transform from the actual set of initial samples S_i in the wavelength scale. Apparently, there is good agreement between $F(l)$ and $F'(l)$ for the low-frequency component with $l = l_{02} = 105$ μm. However, the chirp in $S(\lambda)$ oscillations considered above considerably broadens the spectral components for the high-frequency region, making it rather difficult to determine the positions l_{01} and l_{02} or even resolve them.

Conclusion

We obtained expressions for calculating the spectral characteristics of the interferometer (in reflection mode) for an EFFPI with a multilayer gap within the framework of the Gaussian beam model for radiation propagating in layers, only accounting for single reflections. The properties of such a characteristic and its frequency analysis are considered.

The expressions obtained allow calculating the expected spectral responses of low-finesse multilayer EFFPIs, analyzing their properties and evaluating the key parameters, which is very important to make reasonable choice of the device's parameters and elements to further improve EFFPI-based sensors or construct novel designs.

Appendix 1

The Gaussian beam model has wide application as a solution to the approximate Helmholtz wave equation. This solution corresponds to a paraxial wave propagating along the axis z whose complex amplitude is described by the expression

$$U(z,\rho) = A_0 \frac{W_0}{W(z)} \exp\left[-\left(\frac{\rho}{W(z)} \right)^2 - jkz - j\frac{k \cdot \rho^2}{2R(z)} - j\phi_G(z) \right], \quad \text{(A1-1)}$$

where ρ is the transverse displacement from the axis; k is the wavenumber, $k = 2\pi n/\lambda$ (n is the refractive index of the medium, λ is the radiation wavelength in vacuum); A_0 is the amplitude of the beam determined by the initial conditions; W is the radius (width) of the beam equal to the displacement from the axis at which the amplitude the field drops to the level $1/e$ relative to the maximum on the axis; W_0 is the beam width in the waist, $W_0 = W(0)$; R is the wavefront curvature radius of the beam; φ_G is the Gouy phase charactering an additional phase progression along the beam axis; z is the coordinate ounted from the beam waist.

The so-called Rayleigh beam length r ($r = \pi n W_0^2/\lambda$) can be used to express the dependences of W, R and φ_G on the z coordinate as follows:

$$W(z) = W_0 \sqrt{1 + \left(\frac{z}{r}\right)^2}, \; R(z) = z\left[1 + \left(\frac{z}{r}\right)^2\right], \; \varphi_G(z) = \operatorname{atan}\left(\frac{z}{r}\right). \quad \text{(A1-2)}$$

Appendix 2

The Sellmeier equation for $n(\lambda)$ of silicon takes the following form in the infrared region [23]:

$$n(\lambda) = \sqrt{1 + \frac{a_1\lambda^2}{\lambda^2 - \lambda_1^2} + \frac{a_2\lambda^2}{\lambda^2 - \lambda_2^2} + \frac{a_3\lambda^2}{\lambda^2 - \lambda_3^2}}, \quad \text{(A2-1)}$$

where a_1 = 10.6684293, a_2 = 0.003043475, a_3 = 1.54133408; λ_1 = 0.301516485 μm, λ_2 = 1.13475115 μm, λ_3 = 1104.0 μm.

REFERENCES

1. **Lee B. H., Kim Y. H., Park K. S., et al.,** Interferometric fiber optic sensors, Sensors. 12 (3) (2012) 2467–2486.
2. **Ushakov N., Liokumovich L.,** Resolution limits of extrinsic Fabry–Perot interferometric displacement sensors utilizing wavelength scanning interrogation, Appl. Opt. 53 (23) (2014) 5092–5099.
3. **Fang Z., Chin K. K., Qu R., Cai H.,** Fundamentals of optical fiber sensors. John Wiley & Sons, New York (2012) 395–426.
4. **Rao Y.-J.,** Recent progress in fiber-optic extrinsic Fabry–Perot interferometric sensors, Opt. Fiber Technol. 12 (3) (2006) 227–237.
5. **Pevec S., Donlagić D.,** Multiparameter fiber-optic sensors: a review, Opt. Eng. 58 (7) (2019) 072009.
6. **Sirkis J., Chang C.-C.,** Multiplexed optical fiber sensors using a single Fabry–Perot resonator for phase modulation, J. Light. Technol. 14 (7) (1996) 1653–1663.
7. **Han M., Zhang Y., Shen F., et al.,** Signal-processing algorithm for white-light optical fiber extrinsic Fabry–Perot interferometric sensors, Opt. Let. 29 (15) (2004) 1736–1738.
8. **Arya V., De Vries M., Murphy K. A., et al.,** Exact analysis of the extrinsic Fabry–Perot interferometric optical fiber sensor using Kirchhoff's diffraction formalism, Opt. Fiber Technol. 1 (4) (1995) 380–384.
9. **Wilkinson P. R., Pratt J. R.,** Analytical model for low finesse, external cavity, fiber Fabry–Perot interferometers including multiple reflections and angular misalignment, Appl. Opt. 50 (23) (2011) 4671–4680.

10. **Yu B., Wang A., Pickrell G. R.,** Analysis of fiber Fabry–Pйrot interferometric sensors using low-coherence light sources, J. Light. Technol. 24 (4) (2006) 1758–1767.

11. **Liu G., Han M., Uddin N., Han M.,** Analysis of single-mode fiber-optic extrinsic Fabry–Perot interferometric sensors with planar metal mirrors, Appl. Opt. 60 (26) (2021) 7894–7902.

12. **Martin J., Capmany J.,** Transfer functions of double- and multiple-cavity Fabry–Perot Filters driven by Lorentzian sources, Appl. Opt. 35 (36) (1996) 7108–7111.

13. **Yang Y., Zhang H., Cao G., et al.,** Influence of surface errors on the performance of EFPI based on GRIN lenses, Optik. 125 (14) (2014) 3564–3568.

14. **Gao H., Jiang Y., Cui Y., et al.,** Dual-cavity Fabry–Perot interferometric sensors for the simultaneous measurement of high temperature and high pressure, IEEE Sens. J. 18 (24) (2018) 10028–10033.

15. **Pechstedt R. D.,** Fibre optic pressure and temperature sensor for applications in harsh environments, Proc. SPIE. 8794. Fifth European Workshop on Optical Fibre Sensors, Krakow, Poland (20 May, 2013), (2014) 879405.

16. **Markuse D.,** Loss analysis of single-mode fiber splices, Bell Syst. Tech. J. 56 (5) (1977) 703–718.

17. **Parashar A., Shah A., Packirisamy M., Sivakumar N.,** Three cavity tunable MEMS Fabry Perot interferometer, Sensors. 7 (12) (2007) 3071–3083.

18. **Van de Stadt H., Muller J. M.,** Multimirror Fabry–Perot interferometers, J. Opt. Soc. Am. A. 2 (8) (1985) 1363–1370.

19. **Saleh B. E. A., Teich M. C.,** Fundamentals of photonics, John Wiley & Sons, New York, 1991.

20. **Zhang Y., Li Y., Wei T., et al.,** Fringe visibility enhanced extrinsic Fabry–Perot interferometer using a graded index fiber collimator, IEEE Photonics J. 2 (3) (2010) 469–481.

21. **Ushakov N. A., Liokumovich L. B.,** Investigation of baseline measurement resolution of a Si plate-based extrinsic Fabry–Perot interferometer, Proc. SPIE. 9132. Optical Micro- and Nanometrology (2014) 913214 (1 May 2014).

22. **Diddams S., Diels J.-C.,** Dispersion measurements with white-light interferometry, J. Opt. Soc. Am. B. 13 (6) (1996) 1120–1129.

23. **Grigoriev I. S., Meilikhov E. Z.,** Handbook of physical quantities,1st edition, CRC Press, Boca Raton, Florida, USA, Jan. 25, 1997.

СПИСОК ЛИТЕРАТУРЫ

1. **Lee B. H., Kim Y. H., Park K. S., Eom J. B., Kim M. J., Rho B. S., Choi H. Y.** Interferometric fiber optic sensors // Sensors. 2012. Vol. 12. No. 3. Pp. 2467–2486.

2. **Ushakov N., Liokumovich L.** Resolution limits of extrinsic Fabry – Perot interferometric displacement sensors utilizing wavelength scanning interrogation // Applied Optics. 2014. Vol. 53. No. 23. Pp. 5092–5099.

3. **Fang Z., Chin K. K., Qu R., Cai H.** Fundamentals of optical fiber sensors. New York: John Wiley & Sons, 2012. Pp. 395–426.

4. **Rao Y.-J.** Recent progress in fiber-optic extrinsic Fabry–Perot interferometric sensors // Optical Fiber Technology. 2006. Vol. 12. No. 3. Pp. 227–237.

5. **Pevec S., Donlagić D.** Multiparameter fiber-optic sensors: a review // Optical Engineering. 2019. Vol. 58. No. 7. P. 072009.

6. **Sirkis J., Chang C.-C.** Multiplexed optical fiber sensors using a single Fabry–Perot resonator for phase modulation // Journal of Lightwave Technology. 1996. Vol. 14. No. 7. Pp. 1653–1663.

7. **Han M., Zhang Y., Shen F., Pickrell G. R., Wang A.** Signal-processing algorithm for white-light optical fiber extrinsic Fabry–Perot interferometric sensors // Optics Letters. 2004. Vol. 29. No. 15. Pp. 1736–1738.

8. **Arya V., De Vries M., Murphy K. A., Wang A., Claus R. O.** Exact analysis of the extrinsic Fabry–Perot interferometric optical fiber sensor using Kirchhoff's diffraction formalism // Optical Fiber Technology. 1995. Vol. 1. No. 4. Pp. 380–384.

9. **Wilkinson P. R., Pratt J. R.** Analytical model for low finesse, external cavity, fiber Fabry–Perot interferometers including multiple reflections and angular misalignment // Applied Optics. 2011. Vol. 50. No. 23. Pp. 4671–4680.

10. **Yu B., Wang A., Pickrell G. R.** Analysis of fiber Fabry–Pйrot interferometric sensors using low-coherence light sources // Journal of Lightwave Technology. 2006. Vol. 24. No. 4. Pp. 1758–1767.

11. **Liu G., Han M., Uddin N., Han M.** Analysis of single-mode fiber-optic extrinsic Fabry–Perot interferometric sensors with planar metal mirrors // Applied Optics. 2021. Vol. 60. No. 26. Pp. 7894–7902.

12. **Martin J., Capmany J.** Transfer functions of double- and multiple-cavity Fabry–Perot Filters driven by Lorentzian sources // Applied Optics. 1996. Vol. 35. No. 36. Pp. 7108–7111.

13. **Yang Y., Zhang H., Cao G., Zhao H., Cheng Y.** Influence of surface errors on the performance of EFPI based on GRIN lenses // Optik. 2014. Vol. 125. No. 14. Pp. 3564–3568.

14. **Gao H., Jiang Y., Cui Y., Zhang L., Jia J., Hu J.** Dual-cavity Fabry–Perot interferometric sensors for the simultaneous measurement of high temperature and high pressure // IEEE Sensors Journal. 2018. Vol. 18. No. 24. Pp. 10028–10033.

15. **Pechstedt R. D.** Fibre optic pressure and temperature sensor for applications in harsh environments // Proceedings of SPIE. 2014. Vol. 8794. Fifth European Workshop on Optical Fibre Sensors, Krakow, Poland (20 May, 2013). P. 879405.

16. **Markuse D.** Loss analysis of single-mode fiber splices // The Bell System Technical Journal. 1977. Vol. 56. No. 5. Pp. 703–718.

17. **Parashar A., Shah A., Packirisamy M., Sivakumar N.** Three cavity tunable MEMS Fabry Perot interferometer // Sensors. 2007. Vol. 7. No. 12. Pp. 3071–3083.

18. **Van de Stadt H., Muller J. M.** Multimirror Fabry–Perot interferometers // Journal of the Optical Society of America A. 1985. Vol. 2. No. 8. Pp. 1363–1370.

19. **Салех Б. Е. А., Тейх М. К.** Оптика и фотоника. Принципы и применения. Пер. с англ. 2-е изд. В 2 тт. Долгопрудный: ИД «Интеллект», 2012. Т. 1 – 760 с. Т. 2 – 780 с.

20. **Zhang Y., Li Y., Wei T., Lan X., Huang Y., Chen G., Xiao H.** Fringe visibility enhanced extrinsic Fabry–Perot interferometer using a graded index fiber collimator // IEEE Photonics Journal. 2010. Vol. 2. No. 3. Pp. 469–481.

21. **Ushakov N. A., Liokumovich L. B.** Investigation of baseline measurement resolution of a Si plate-based extrinsic Fabry–Perot interferometer // Proceedings of SPIE. 2014. Vol. 9132. Optical Micro- and Nanometrology. P. 913214 (1 May 2014) 6 p.

22. **Diddams S., Diels J.-C.** Dispersion measurements with white-light interferometry // Journal of the Optical Society of America B. 1996. Vol. 13. No. 6. Pp. 1120–1129.

23. **Григорьев И. С., Мейлихов Е. З.** Физические величины. М.: Энергоатомиздат, 1991. 1232 с.

THE AUTHORS

LIOKUMOVICH Leonid B.
Peter the Great St. Petersburg Polytechnic University
29 Politechnicheskaya St., St. Petersburg, 195251, Russia
leonid@spbstu.ru
ORCID: 0000-0001-5988-1429

USHAKOV Nikolai A.
Peter the Great St. Petersburg Polytechnic University
29 Politechnicheskaya St., St. Petersburg, 195251, Russia
n.ushakoff@spbstu.ru
ORCID: 0000-0002-3480-2779

MARKVART Aleksandr A.
Peter the Great St. Petersburg Polytechnic University
29 Politechnicheskaya St., St. Petersburg, 195251, Russia
markvart_aa@spbstu.ru
ORCID: 0000-0001-8080-0830

EVDOKIMENKO Ekaterina Yu.
Peter the Great St. Petersburg Polytechnic University
29 Politechnicheskaya St., St. Petersburg, 195251, Russia
evdokimenko.97@inbox.ru
ORCID: 0000-0001-7739-9898

СВЕДЕНИЯ ОБ АВТОРАХ

ЛИОКУМОВИЧ Леонид Борисович – *доктор физико-математических наук, профессор Высшей школы прикладной физики и космических технологий Санкт-Петербургского политехнического университета Петра Великого.*
195251, Россия, г. Санкт-Петербург, Политехническая ул., 29
leonid@spbstu.ru
ORCID: 0000-0001-5988-1429

УШАКОВ Николай Александрович – *кандидат физико-математических наук, доцент Высшей школы прикладной физики и космических технологий Санкт-Петербургского политехнического университета Петра Великого,* Санкт-Петербург.
195251, Россия, г. Санкт-Петербург, Политехническая ул., 29
n.ushakoff@spbstu.ru
ORCID: 0000-0002-3480-2779

МАРКВАРТ Александр Александрович – *ассистент Высшей школы прикладной физики и космических технологий Санкт-Петербургского политехнического университета Петра Великого.*
195251, Россия, г. Санкт-Петербург, Политехническая ул., 29
markvart_aa@spbstu.ru
ORCID: 0000-0001-8080-0830

ЕВДОКИМЕНКО Екатерина Юрьевна – *аспирантка Высшей школы прикладной физики и космических технологий Санкт-Петербургского политехнического университета Петра Великого.*
195251, Россия, г. Санкт-Петербург, Политехническая ул., 29
evdokimenko.97@inbox.ru
ORCID: 0000-0001-7739-9898

Received 14.10.2022. Approved after reviewing 23.10.2022. Accepted 23.10.2022.
Статья поступила в редакцию 14.10.2022. Одобрена после рецензирования 23.10.2022. Принята 23.10.2022.